行政院國家科學委員會專題研究計畫　成果報告

子計劃二：光晶球體及半導體毫微米晶粒之鑑測研究部制

(2/2)

計畫類別：整合型計畫
計畫編號：NSC91-2120-E-002-008-
執行期間：91 年 08 月 01 日至 93 年 07 月 31 日
執行單位：國立臺灣大學化學系暨研究所

計畫主持人：張哲政

計畫參與人員：(研究助理)

報告類型：完整報告

處理方式：本計畫可公開查詢

中　華　民　國 93 年 12 月 10 日

行政院國家科學委員會專題研究計畫完結報告

奈米光粒子合成,能隙晶體結構製作與應用—
子計劃二:光晶球體及半導體毫微米晶粒之鑑測研究

計畫編號：**NSC91-2120-E-002-008**
執行期限： 91 年 8 月 1 日至 93 年 7 月 31 日
主持人： 張哲政
執行機構及單位：臺灣大學化學系

Introduction

The end of the twentieth century was marked by the astonishing advances in semiconductors, which transformed the communications and computing industries by channeling electrons faster than the large old vacuum tube could. In a semiconductor crystal such as silicon, the atoms are arranged in a lattice structure of periodic potentials. When electrons moving through the lattice and interact with the silicon nuclei, they experience the periodic potential. This interaction causes the formation of allowed and forbidden energy states. For pure and perfect crystals, no electrons are allowed to occupy the energy states in an energy range called the forbidden energy gap. For real materials, the periodicity of the lattice is perturbed either by the missing of the lattice atom, by the replacement of the lattice atom by an impurity atom, or by incorporation of the impurities at interstitial sites. In this case, .electrons can have an energy within the band gap. The control of the energy costs for electron transiting between the band gap led to the flourishing the semiconductor industry in the second half

Many scientists expect that the semiconductor industry will be transformed in the 21st century by photonic crystals, which relies on the similar periodic potential of the latticelike structures to manipulate photons as semiconductors do to the electrons. The striking advantages are, however, associated with at the speed of light and the lack of resistance when photons flow. The primitive photonic crystal contains a number of tiny air holes, which are arranged in a lattice pattern with. regions of high refractive index interspersed with regions of low refractive index. The high refractive index material is dielectric material and the low one the air holes. The contrast in refractive index renders photons to experience a periodic potential just like what the electrons experience when they travel through the silicon crystal. Similarly to the band gap formed in the semiconductor crystal for electrons, a photonic band gap (PBG) will form in a patterned dielectric material of two regions having large contrast in refractive index.

Photonic band gap crystals are thus expected to function like optical analogs of semiconductors. Just as the presence of an energy band gap prohibits electrons with certain energies to move through a semiconductor, the existence of an optical frequency band gap will prevent light of certain frequencies to propagate through PBG crystals. The difference of these two band gaps is that the semiconductor band gap is due to the electronic structure of the material, whereas the PBG band gap is caused by the crystal structure. Depending on the details of the crystal structure, light of certain wavelengths can be strongly scattered. For example, if an excited molecule which can emits blue light is trapped inside a PBG crystal that has a blue photonic band gap, the molecule would remain in the excited state indefinitely because the blue photon can go nowhere. The blue light can be emitted only if the PBG crystal is disturbed (for example, by a pulse of sound waves) such that the crystal lattice parameters are changed. The position of its photonic band gap is shifted to a slightly different frequency and this allows the blue light to emit.

The technologies of fabricating dielectric materials of specific photonic band gaps and of shifting the position of the photonic band gap are not as well developed, however, as the one in the semiconductor industry. With the semiconductors, the electron flow is controlled by a combination of dopants and applied voltage. The flow of electrons can be controlled easily to switch on and off particular electrical functions using the sophisticated technologies developed. By selectively sending current through a circuit at specific time, signals for performing designed functions can be manipulated. At present, particular functions cannot be controlled easily using light in the similar way, however. There is no active method available to completely stop and release a light beam, which, under the present technology, can only be redirected using lenses, mirrors, and fibers. With the great potential of actively controlling light, PBG crystals are actively sought.

Several different synthesis/construction routes have been proposed for obtaining the PBG structures of specific properties. Artificial opals made by means of sedimentation of SiO2 nanospheres in an ordered fashion have been shown to be excellent candidates to build up 3D photonic crystals.[1] Other methods include micromachining of a bulk material by lithographic methods, layer by layer stacking using lithography, and wafer bonding. Recently, autocloning technology was proposed for fabricating multidimensional PBG crystals.[2,3] This technology is based on the deposition of multiplayer wavy films onto a substrate with periodically-arrayed holes or grooves by a combination of radio-frequency sputtering and an etching process.

Among the construction routes that have been proposed for obtaining the PBG structures, natural sedimentation of silica spheres is probably one of the most studied method. It has been confirmed that solid colloidal PBG crystals made of submicrometer SiO2 spheres are packed in a face centered cubic (fcc) lattice.[4,5] Questions remain as to the detailed procedure for fine tuning the PBG properties of 3D crystalline arrays that were assembled from nanometer-sized beads. For example, it was predicted[6] that synthetic opals made by SiO2 can have a complete photonic band gap. The PBG properties of opals can be varied by changing the sphere diameter so as to cover the visible and near-IR region of the spectrum.[7] Its properties can be further modified by capping the spheres with organic materials, filling the voids with another material or adjusting the SiO2/air volume fraction.[8] Usually, the filling factor, defined as the ratio between the volume occupied by the SiO2 spheres and the total volume of the structure, could be controlled by thermal annealing.[9.10] It is worthy to point out that, as supported by light transmission and reflection measurements, the variation in the optical properties of SiO2 colloidal PBG crystals, when they are thermally treated, is not due to a loss of order, but to structural and physicochemical modifications of the material caused by thermal annealing.[11]

Exact characterization of the physical and chemical properties of the constituent spheres and the assembled PBG crystals holds the promise of further advancing this novel material to its full potential in device application. In the case when the optical properties of SiO2 colloidal PBG crystals is varied through thermal treatment, determination of optical properties of PBG structures by means of light transmission and reflection measurements has shown that the optical variation is not due to a loss of order, but to structural and physicochemical modifications of the material caused by thermal annealing.[12] By systematically comparing properties of the spheres synthesized under various conditions, the chemical and physical characterization provides useful information about key factors controlling the thermal stability, chemical inertness, porosity, density, composition, and structural rigidity of the sphere.

Surface characterization of the intermediates formed in above-mentioned organic templating methods is essential to the continued development of the organic templating method for preparing high-quality holey materials for real optoelectronics application. The presence of impurity in the holey structure will alter the refractive contrast of the material, and result in a change of the photonic behavior of the holey materials. The macroporous materials generated from the organic templating method so far can only prevent light from traveling in half of the possible directions.[13] Chemical analysis has shown that the carbon content of the calcined samples varies substantially, indicating that the extent of removal of the latex templates from the 3D host may depend on the details of the organic templating procedure, especially on the heat treatment. Proper chemical-state imaging analysis is thus essential in providing valuable information about the origin and the chemical mechanism of formation of the impurity. The chemical-state imaging capability is also essential in revealing the evolution of the semiconductor nanoparticles depositing and growing on the constituent spheres of the PBG crystals.

Experiment

In the past few years, we have developed PBG spheres using the Stober method, which allows the chemical transformation of TEOS to take place in ethanol under the catalysis of ammonia, as described in the following equations:

—Si-OR + H_2O ⟶ —Si-OH + ROH
—Si-OR + —Si-OH ⟶ —Si-O-Si— + ROH
—Si-OH + HO-Si— ⟶ —Si-O-Si— + H_2O

The overall reaction thus is:

$Si(OR)_4 + 2H_2O \longrightarrow SiO2 + 4ROH$

The synthesis experimental conditions were tests by varying the concentration of various key chemicals and by changing the reaction temperature. Optimal synthesis approach was then developed.

In addition, efforts were directed toward understanding the reaction mechanism involved in the synthesis. In particular, the role of the solvent molecule on the silica sphere chemical properties was address. This aspect of the experiments was conducted in a well controlled condition simulating the reaction taking place involving the sole partners of the molecule/solid of interest. Experiments were performed in a stainless steel ultrahigh vacuum system with a background pressure typically of 2×10^{-10} torr. The details of our system design are described elsewhere.[14] Briefly, the system is pumped by a 500 L/s turbomolecular pump and equipped for temperature-programmed desorption (TPD), static secondary ion mass spectrometry (SSIMS), Auger electron spectroscopy (AES), and low-energy electron diffraction (LEED).

The reaction mechanism study was conducted on silicon dioxide samples, which were prepared using n-type (Sb-doped, $\rho = 0.0001 – 0.02\ \Omega$-cm) Si(100) wafers acquired from International Wafer Service. After cleaved into approximately 12 mm x 8 mm x 0.5 mm rectangles, they were subjected to a wet-chemical cleaning process[15] to remove grease left on the sample. Silicon dioxide was then grown on the Si(100) surface by thermal oxidation in an oven at an elevated temperature of ~750 ℃ in air for six hours. The thickness of the silicon dioxide layer formed was ~100 Å, as revealed from the depth profiling of the sample surface using x-ray photoelectron spectroscopy. After the growth, the sample was placed in a pocket of the thin tantalum sheet, which provided the thermal and electrical conductions as well as the mechanical support for the sample, and mounted to a manipulator using tantalum clamps. A pair of Chromel-Alumel thermocouples was spot-welded to the pocket for monitoring the sample temperature. Once under ultrahigh vacuum, the sample surface was cleaned by cycles of Ar^+ ion sputtering (2 keV, 0.6 μA beam current, 1-2 x 10^{-6} torr, 10 min) and annealing (700 ℃, 1 min). Surface cleanliness of the sample was checked by AES and SSIMS.

To study the solvent chemical effect on the growth of PBG spheres of silica, ethanol (99.5%) was employed, which was purchased from Acros and deuterated ethanol (C_2D_5OD, >99%) from CIL. Prior to dosing, these chemicals were degassed by several freeze-pump-thaw cycles. A stainless steel gas doser of 2 mm i.d. was used to introduce them onto the sample in the UHV chamber through a precision leak valve. The purity of the ethanol vapor was checked in situ by mass spectrometry. All doses reported in this study are calibrated back to the background exposure and are expressed in langmuirs (1 L = 1 x 10^{-6} torr-s) of exposure at the sample surface. In the study, SSIMS measurements were performed using a primary beam of Ar^+ ions of 2 keV energy to bombard the sample, with the angle between the ion gun and the mass spectrometer fixed at 45 degrees. The ion gun was differentially pumped and operated at a pressure of ~3 x 10^{-9} torr when SSIMS spectra were recorded. The count rate of secondary ions was maximized by varying the polar angle of ion incidence and by applying a bias voltage (~20 V) on the sample. Data collection was accomplished using an interface system designed by VG Microtech. In addition, TPD experiments were conducted with the sample in line-of-sight of the mass spectrometer (non-differentially pumped). To preferentially admit gases desorbing directly from the sample surface to the ionizer, this spectrometer was fitted with a stainless steel skimmer with a 0.3 cm. diameter opening. For TPD measurements, the sample was placed ~0.1 in. away from the skimmer. Measurements of the intensities of desorbing species were controlled by interfacing the spectrometer control unit to a personal computer. During each TPD measurement, a linear temperature ramp was applied to the sample and the spectrometer was set to monitor several masses. A heating rate of ~3 ℃/s was used in all TPD experiments.

Results and Discussion

One of the key issues involved in obtaining silica opal of good quality is to synthesize silica spheres of uniform diameters and high purity. Examples of the SEM images of the spheres obtained are shown in Fig. 1a and 1b.

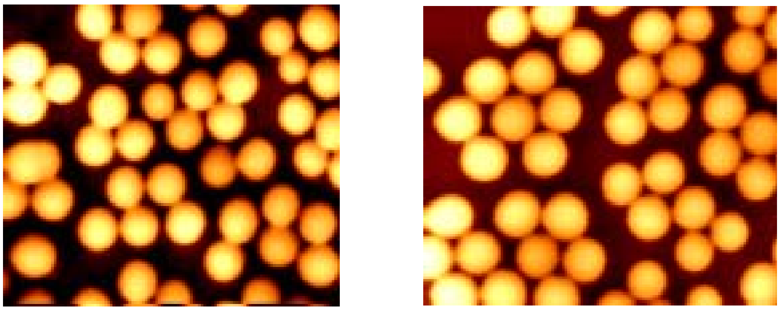

Fig. 1 SEM images obtained from PBG spheres of silica prepared using the Stober method after a reaction time of (a) 3 and (b) 4 hours.

The spheres shown in Figs 1a and 1b were obtained with reaction temperature of 0C and reaction time of 3 and 4 hours, respectively. The reaction stoichiometry of the synthesis was examined by systematically changing the amount of one chemical while allowing the amounts of other chemicals invaried. The dependence of the TEOS concentration on the sphere diameter was obtained as follows:

Name	TEOS(M)	NH3(M)	H2O(M)	Average diameter (nm)	Standard deviation
Teos2	0.26	0.24	6.66	143	5.413
Teos4	0.35	0.24	6.66	156	5.04
Teos6	0.53	0.24	6.66	164.6	9.62
Teos8	0.7	0.24	6.66	214	8.73
Teos10	0.88	0.24	6.66	223	8.96

In addition, the effect of the amount of water used in the reaction chamber to the size of the sphere synthesized is as follows:

Name	TEOS(M)	NH3(M)	H2O(M)	Average diameter (nm)	Standard deviation
H2O6	0.26	0.4	6.66	418.23	6.87
H2O8	0.26	0.4	8.88	526.38	8.48
H2O10	0.26	0.4	11.1	563.38	9.12
H2O12	0.26	0.4	13.3	384	8.76

Changing the concentration of the ammonia in the reaction chamber also causes the change of the sphere diameter, as shown in the flowing table:

Name	TEOS(M)	NH3(M)	H2O(M)	Average diameter (nm)	Standard deviation
NH34	0.35	0.04	4.45	41.76	4.44
NH36	0.35	0.08	4.45	57.09	6.98
NH38	0.35	0.16	4.45	78.23	7.56
NH310	0.35	0.24	4.45	95.92	8.88
NH312	0.35	0.32	4.45	125.24	9.57
NH314	0.35	0.40	4.45	131.23	9.73

Examples of the repeatability and the stirring rate on the silica sphere of a particular diameter are shown in the following table, in which the Ran C and Run D were obtained using different stirring rates:

Name	*TEOS(M)*	*NH3(M)*	*H2O(M)*	*Average diameter (nm)*	*Standard deviation*
A	0.7	0.24	4.45	286.3396	7.69
B	0.7	0.24	4.45	288.36	10.73
C	0.35	0.32	8.88	90.51	7.86
D	0.35	0.32	8.88	86.88	8.98

The effect of reaction temperature on the diameter of the silica spheres synthesized was also examined. The SEM images obtained for spheres obtained at the reaction temperatures of 50 C, 40 C, 21.5 C and 0.0 C are shown in Figs. 2, 3, 4, and 5, respectively.

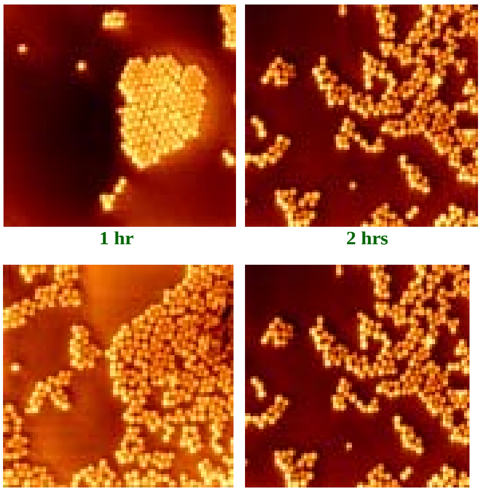

1 hr

2 hrs

3 hrs

4 hrs

Fig. 2 SEM images obtained from PBG spheres of silica prepared using the Stober method after the indicated reaction times and a reaction temperature of 50 C

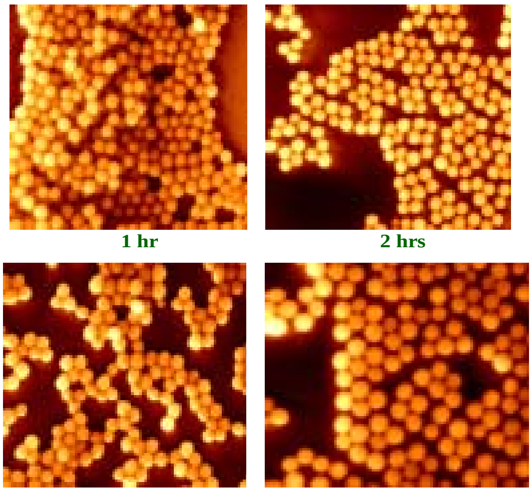

1 hr

2 hrs

3 hrs

4 hrs

Fig. 3 SEM images obtained from PBG spheres of silica prepared using the Stober method after the indicated reaction times and a reaction temperature of 40 C.

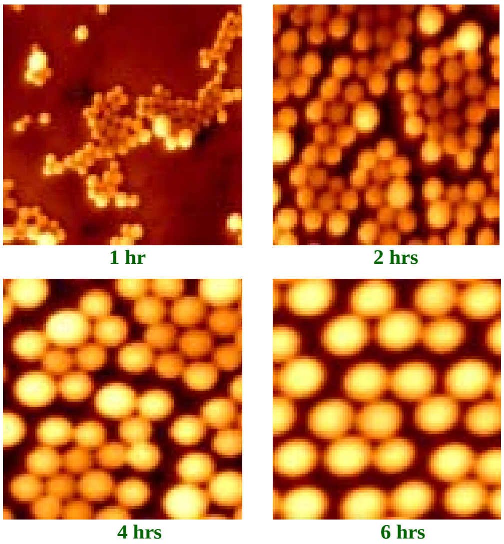

Fig. 4 SEM images obtained from PBG spheres of silica prepared using the Stober method after the indicated reaction times and a reaction temperature of 21.5 C

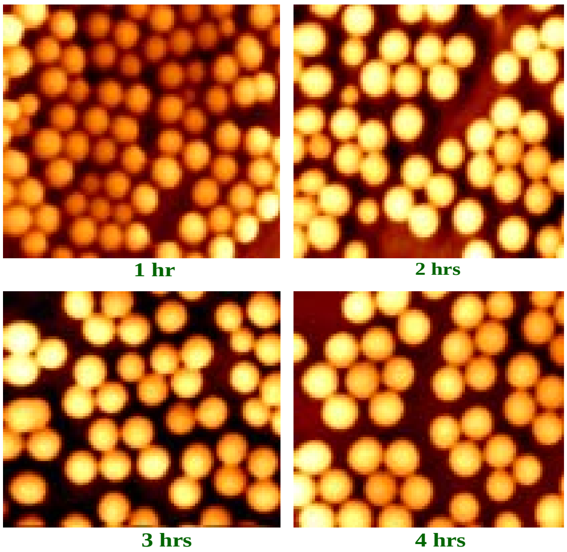

Fig. 5 SEM images obtained from PBG spheres of silica prepared using the Stober method after the indicated reaction times and a reaction temperature of 0 C. The images obtained at 3 hrs and 4hrs are reproduced from Fig. 1 for better comparison

The silica spheres synthesized were then deposited on ITO and the 3D PBG crystals obtained were analyzed using various analytical methods. Fig 5. shows the PBG crystals obtained using 260 nm silica particles, which shows an unique greenish color.

Fig. 6 Three-dimensional PBG crystals prepared from 260 nm silica spheres.

Further study was carried out to address the following questions related to the effect of solvent molecules on the formation of the PBG spheres using the metal-free, high-purity silicon dioxide surface as a model: i) Does ethanol decompose on the metal-free silicon dioxide surface? ii) If it does, to what extent do ethanol molecules decompose and what are the identities of their decomposition products? iii) How are some of these products formed during the ethanol reaction on silicon dioxide (i.e., which chemical bonds in ethanol are disrupted during the reaction and which new bonds are formed on the surface)? iv) What are the hydrogen-containing species produced from ethanol reactions on silicon dioxide?

The surface reaction of ethanol on the silicon dioxide surface at low temperature was studied using static secondary ion mass spectrometry. The substrate temperature for these SSIMS experiments was maintained at –160 ℃. The SSIMS spectra taken up to m/e 55 by exposing several different doses of EtOH to the silicon dioxide surface prepared are shown in Fig. 7. Results of the comparison study the SSIMS spectra taken from the silicon dioxide surface exposed at –160℃ to the indicated doses of deuterated ethanol, C_2D_5OD (d-EtOD) are shown in Fig. 8. A typical SSIMS spectrum measured from the surface after cycles of sample cleaning showed peaks at m/e 28, 40, 44, and 45. The m/e 28 peak arose from the sputter desorption of Si^+ ions from the surface, as supported by the presence in the spectrum of small m/e 29 and m/e 30 peaks due to the presence of Si isotopes in nature. Since the sputter yield generally decreases drastically with the layer depth of atoms sputtered from the surface,[16-18] the large signal, relative to other peaks in the spectrum, observed at m/e 28 before EtOH exposure reveals that the Si atoms in the sample surface were not completely buried under oxygen atoms. The exposed Si atoms on the surface may facilitate the reactions of ethanol with silicon dioxide following ethanol adsorption, as will be discussed later.

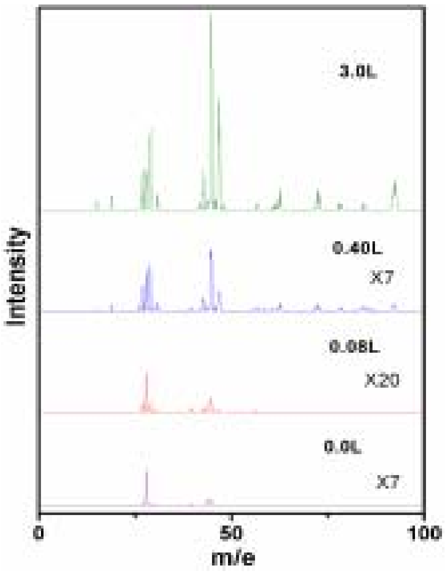

Fig. 7 SSIMS spectra obtained from the silica sample surface exposed to the indicated doses of ethanol..

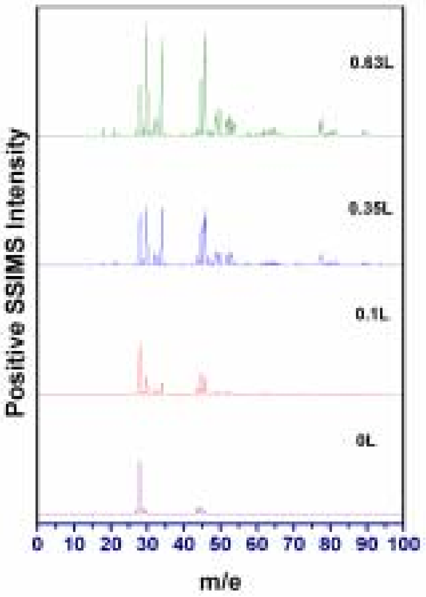

Fig. 8 SSIMS spectra obtained from the silica sample surface exposed to the indicated doses of deuterated ethanol..

Fig. 7 shows that the sputter intensity measured at m/e 44 did not increase with the ethanol dose in the low exposure regime. Instead, its peak area remained at about a constant ratio (19±2%) of the one obtained at m/e 28. The m/e 44 peak thus reflects the characteristics of the sample surface, not of the ethanol reaction on silicon dioxide. It was assigned as due to SiO^+ ions sputtered from the surface. The absence of SSIMS peaks in Fig. 7 from sputtering of low ionization-potential elements, such as Na and K, indicates that the impurity level of metals in the sample prepared was below the detection limit of SSIMS.

The presence of m/e 45 signals in Fig. 7 and m/e 46 peaks in Fig. 8 revealed the formation of hydroxyl functional group on the silica surface. It should be pointed out that hydroxyl groups are usually present on all the surface of solid oxides unless the surface is treated at elevated temperatures[19] or the dissociative adsorption of water on the oxide surface is a kinetically hindered process.[20] These groups may behavior as hydrogen bond donors or proton donors (Bronsted acid), depending on their coordination symmetry.[21] They affect the reactivity of the oxide sample significantly.[22]

For better understanding the reaction process involved in the reaction of the solvent on the PBG spheres of silica, the assignments of the main peaks observed in Figs. 7 and 8 are summarized in Table I. These assignments are supported close comparison of the intensity variation of the related peaks with the exposure. For example, as shown in Fig. 8, there was a substantial increase in the SSIMS intensity observed at m/e 30 at the d-EtOD exposure of 0.1L, as compared to its intensity obtained before exposure. Major SSIMS signals were also detected at m/e 34 and m/e 46. In comparison to the SSIMS spectra taken from the sample surface exposed to EtOH (Fig. 7), it indicated that the m/e 30 peak was related with the sputtering of $C_2D_3^+$ ions, the deuterated counterpart of the m/e 27 species appearing in Fig. 7, and the m/e 34 peak with that of deuterated ethyl ions. The rise of small peaks at m/e 33 and m/e 32 in Fig. 8 may be ascribed in part to isotope exchange of D from $CD_2CD_3^+$ with H on the surface. The occurrence of the H/D exchange reaction on the surface at the low d-EtOD exposure of 0.1L suggests that a noticeable amount of hydrogen atoms was present on the sample surface prepared in this study before ethanol exposure.

TABLE 1: Assignments of SSIMS Signals Observed in the Spectra Taken from the Silica Surface Exposed to EtOH and d-EtOD, Respectively

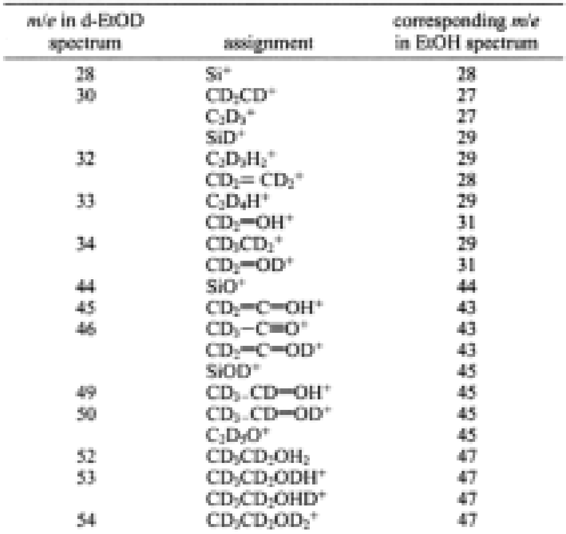

m/e in d-EtOD spectrum	assignment	corresponding *m/e* in EtOH spectrum
28	Si^+	28
30	CD_2CD^+	27
	$C_2D_3^+$	27
	SiD^+	29
32	$C_2D_3H_2^+$	29
	$CD_2{=}CD_2^+$	28
33	$C_2D_4H^+$	29
	$CD_2{=}OH^+$	31
34	$CD_3CD_2^+$	29
	$CD_2{=}OD^+$	31
44	SiO^+	44
45	$CD_2{=}C{=}OH^+$	43
46	$CD_3{-}C{\equiv}O^+$	43
	$CD_2{=}C{=}OD^+$	43
	$SiOD^+$	45
49	$CD_3{-}CD{=}OH^+$	45
50	$CD_3{-}CD{=}OD^+$	45
	$C_2D_5O^+$	45
52	$CD_3CD_2OH_2$	47
53	$CD_3CD_2ODH^+$	47
	$CD_3CD_2OHD^+$	47
54	$CD_3CD_2OD_2^+$	47

The reverse in relative sputter intensities of $C_2X_3^+$ and $C_2X_5^+$ ions (X = D or H) shown in Figs. 7 and 8 thus supports the argument that, in addition to those already exist before exposure, new Si-X bonds may be formed on the silicon dioxide surface exposed to ethanol. The sputtering of SiX^+ (X = D or H) ions disclosed in these two figures, however, could result from the recombination reactions, occurring in the space above the surface, of the desorbed Si and X atoms which were emitted from the sample surface via certain correlated collision sequences.[23-25] In order to confirm that the observed SiX^+ ion sputtering was mainly due to the formation of Si-X bonds on the surface exposed to ethanol, estimation on the contribution of SiX^+ ions to the intensities measured at m/e 29 in Fig. 7 and at m/e 30 in Fig. 8 was performed. The estimation was based on the assumption that the m/e 32, m/e 33, and m/e 34 peaks observed in Fig. 8 were contributed from ethyl ions alone and that the relative abundance of C_2X_3 and C_2X_5 remained about the same in the ethanol exposure range between 0.30L and 0.35L. The areas of the m/e 27 and m/e 29 peaks obtained at 0.40L EtOH exposure (Fig. 7) and of the m/e 30, m/e 32, m/e 33, and m/e 34 peaks measured at 0.35L d-EtOD exposure (Fig. 8) were each calculated. The difference and reversal in the intensities observed in Figs. 7 and 8 between C_2X_3 and C_2X_5 were then used to estimate their contributions from SiX^+ ion sputtering.

The results indicated that SiD^+ ions sputtered from the surface contributed significantly to the m/e 30 signal intensity (~51%) shown in Fig. 8 at 0.35L exposure, after the contribution due to the presence of residual ^{29}SiH species on the surface was removed. A large contribution of ~32% was obtained for SiH^+ ions to the m/e 29 SSIMS intensity shown in Fig. 7 at 0.40L exposure. Comparison with their corresponding Si^+ SSIMS intensities revealed that these calculated SiX^+ intensities were significantly higher than the predicted values for ion formation via space recombination,[23-25] if the ionization probabilities of Si and SiH during sputtering were assumed similar. Therefore, an appreciable number of Si-H bonds were formed on silicon dioxide during ethanol decomposition on the surface. The observation on the formation of new Si-H bonds from hydrogen atoms produced during ethanol dissociation on silicon dioxide is in agreement with conclusions from an earlier report that hydrogen atoms are highly mobile in the oxide and diffuse through it toward the silicon-silicon oxide interface where they create defects.[26]

Our results also confirm that on silicon dioxide, the Et-OH bond may be cleaved and ethanol may decompose to the extent that ethyl species are produced. As shown in Figs. 7 and 8, the abundance of C_2H_3 and C_2D_3 on the surfaces reacted with EtOH and d-EtOD, respectively, reveals that the C-X (X = D or H) bond in the ethyl group may be also disrupted during ethanol reaction with silicon dioxide. The H (or D) atoms produced from the disruption may then aid in the formation of the Si-H bonds.

The attributions made above are supported by the SSIMS spectra taken from the silicon dioxide surface exposed to deuterated ethanol. At the d-EtOD exposure of 0.1L, the SSIMS spectrum obtained, shown in Fig. 8, exhibited a large increase in intensity at m/e 45 and m/e 46, in addition to the rise of sputter intensities at m/e 49, 50, 52, 53, and 54. The m/e 54 peak corresponds to the peak observed at m/e 47 in Fig. 7. It arose from the sputter desorption of the d-EtOD molecule from the sample in the form of d-$EtOD_2^+$ after acquiring a D atom from the silicon dioxide surface. Since at the low d-EtOD exposure of 0.1L, the sample surface was populated with H species, as discussed above, the d-EtOD molecule on the surface may acquire a H atom, instead, from the surface during its sputter desorption. The m/e 53 (d-$EtODH^+$) peak was thus observed and its signal intensity was larger than the one measured at m/e 54.

The presence of a relatively large peak at m/e 52, in comparison to the m/e 53 and m/54 peak intensities, in Fig. 8 is very interesting. The much smaller signal intensity observed at m/e 46 than at m/e 47 in Fig. 7 excludes the possibility that deuterated ethanol was sputtered mainly in the form of d-$EtOD^+$ (m/e 52). The smaller peaks observed at m/e 33 and 32 than the one at m/e 34 in Fig. 8 reveal that H/D exchange of adsorbed species with surface H atoms is kinetically suppressed to some extent. The m/e 52 species present in a relatively large amount were thus not produced mainly from H/D exchange of the m/e 54 or m/e 53 species. The relatively large SSIMS intensity observed at m/e 52 also does not warrant the formation of the m/e 52 species via simultaneous acquisition of two H atoms from the sample surface by the m/e 50 species during sputter desorption, either. Therefore, a species in the form of C_2D_5HO (i.e., d-EtOD with one D being replaced by H) had to be present on the surface, which then acquired a H atom during sputtering from the surface to desorb as m/e 52.

Instead of H/D exchange between the surface H atoms and the ethanol D atoms on hydroxyls, which was kinetically suppressed to some extent, as pointed out earlier, such a substitution reaction was facilitated by the presence of silanols on the sample surface. As discussed before, the presence of the m/e 45 peaks with distinctive intensities at 0L exposure in Figs. 7 and 8 indicates that a discernible amount of silanols were present on the silicon dioxide surface prior to ethanol exposure. The substitution reaction may take place via hydrogen bonding between the silanol on the surface and the hydroxyl group of ethanol,[27,28] as illustrated in Fig. 9. It leads to the production of C_2D_5HO (d-EtOH) and deuterated silanol (SiOD). The production of SiOD contributes in part to the large increase in SSIMS intensity observed at m/e 46 in Fig. 8 at increasing exposures.

As shown in Fig. 8, the two pairs of SSIMS peaks, one present at m/e 49 and m/e 52 and the other at m/e 50 and m/e 53, display similar intensity ratios at each ethanol dose. The peaks observed at m/e 49 and 52 may be due to surface reactions originating from an identical compound, d-EtOH, and the peaks at m/e 50 and 53 originating mainly from d-EtOD in the low exposure regime, as discussed above and depicted in the equations below.

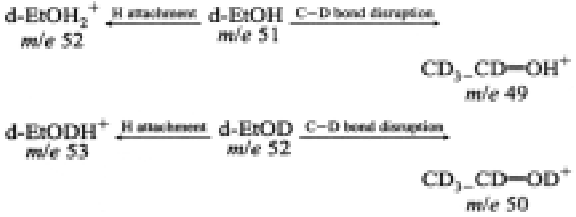

The similarity thus supports that the m/e 50 SSIMS intensity was mainly contributed from CD_3-CD=OD$^+$ ions. The contribution of d-EtO$^+$ to the m/e 50 peak intensity shown in Fig. 8, and thus of EtO$^+$ to the m/e 45 intensity in Fig. 7, is minor. This conclusion is in agreement with the results obtained from ab initio calculations,[29] which showed that out of the three stable isomers of $C_2H_5O^+$ (i.e., EtO$^+$), the 1-hydroxylethyl (CH_3CHOH^+) cation was more stable than the ethoxy and 2-hydroxyethyl ($CH_2CH_2OH^+$) cations.

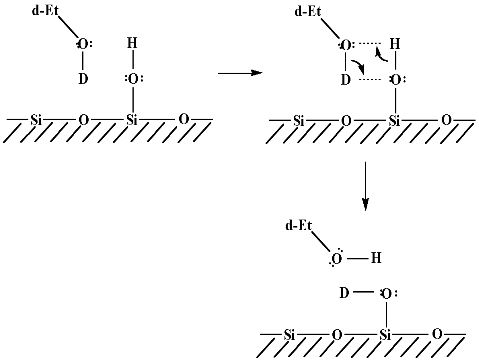

Fig. 9 Illustration of a possible substitution reaction via hydrogen bonding between silanol on the surface and the hydroxyl group of ethanol..

The minimal contribution of d-EtO$^+$ ions to the m/e 50 peak intensity shown in Fig. 8 does not imply that the EtO population on the silicon dioxide surface exposed to ethanol at -160℃ is negligible. On the contrary, it may constitute one of the major products yielded from ethanol decomposition on the surface. Early studies of ethanol reactions occurring at different temperatures above 180℃,[30-32] on the silica surface have found that ethoxy was formed on the surface, with a density as high as twice the hydroxyl surface density.[32] Its decomposition was believed to produce ethylene detected at high substrate temperatures.[31] For the case of methanol exposure to silica, methoxy groups were also formed on the surface.[33] The lack of the EtO$^+$ contribution to SSIMS signals observed in Figs. 7 and 8 may be due to the energetics associated with the homolysis of the EtO-Si bond following ion irradiation. The energy of 1.712 eV[34,35] is released when an electron is added to ethoxy to form EtO$^-$, whereas the energy of 10.29 eV[36] is required if the outermost electron is to be removed from ethoxy to form EtO$^+$. The chance of detecting EtO$^+$ in the positive SSIMS is thus greatly reduced.

Fig. 10 shows the variation in the peak area of some major SSIMS peaks obtained from increasing doses of EtOH. It revealed that ethoxy was present on the sample surface exposed to ethanol at –160℃. Presented in Fig. 10 is the variation in the peak area of some major SSIMS peaks obtained from increasing doses of EtOH. As shown in the figure, the areas of all peaks increase rapidly with the ethanol coverage in the low exposure regime of less than ~0.5L. At higher exposures, the rate of increase diminishes in the log scale until the exposure of ~2L, after which the rates for all signals except m/e 47 become similar and small. The m/e 47 peak area, however, continues to increase with the ethanol exposure. The continuous, large increase in the SSIMS intensity for m/e 47 ($EtOH_2^+$) at increasing ethanol exposures shows that at high exposures, ethanol physisorbs in the molecular form on the silicon dioxide surface at –160℃ via hydrogen bonding. Similar observations were also obtained from FTIR studies of ethanol on the silica surface.[37]

If both the m/e 46 and m/e 47 peaks in Fig. 7 are brought about from ethanol molecules adsorbed on the surface, one would expect to observe similar dependence of their peak areas on the exposure. The absence in Fig. 10 of a continuous, large increase in the m/e 46 SSIMS peak area with the exposure indicates that the m/e 46 peak observed in Fig. 7 can not be attributed to ethanol present in the molecular form on the surface. It is thus postulated that ethoxy groups was present on the sample surface exposed to ethanol at –160℃ and bonded to the silicon atoms exposed to vacuum. Ion bombardment initiated collision cascades leading to the breakage of the EtO-Si bond. The ethoxy species produced was then protonated to contribute to the m/e 46 ($EtOH^+$) signal observed in Fig. 7. The change in the SSIMS peak area for m/e 46 with the exposure thus follow the same pattern, as shown in Fig. 10, as those displayed by the surface species produced by ethanol reactions on silicon dioxide.

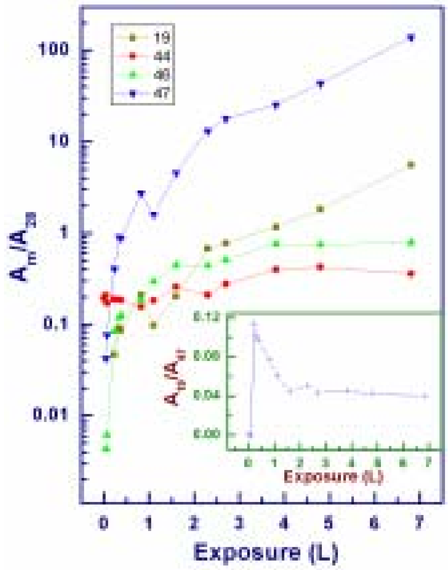

Fig. 10 Ratios, displayed on the log scale, of peak areas obtained at m/e 19, 44, 46, and 47 to the area of the m/e 28 peak in the SSIMS spectra of a silicon dioxide surface exposed to EtOH. All measurements were taken at –160 ℃. Inset: Same ratios displayed on the linear scale.

Once formed, the ethoxy groups on silicon atoms can interact and form a hydrogen bond through its oxygen atom, fixed at a distance close to the surface, with a neighboring isolated OH group, producing a stable associated species.[30] Infrared studies of the reaction of methanol on silica have also established such interaction to be predominant between surface silanols and the adsorbed species.[27] Ethoxy may thus be present on the silicon dioxide surface with a notable density following ethanol reactions.[32]

The presence of silanol groups on the bare sample surface, before the exposure of deuterated ethanol, resulted in a significant contribution of $SiOH^+$ to the signal intensity measured at m/e 45 at low d-EtOD exposures. It caused the m/e 45 intensity to be higher than that the m/e 46 intensity observed at 0.1L exposure in Fig. 8. As the relative concentration of surface H atoms was decreased with increasing d-EtOD exposures, less d-EtOH was produced. It in turn caused the relative surface concentrations of d-$EtOH_2^+$ (m/e 52), CD_3-CD=OH^+ (m/e 49) and CD_2=C=OH^+ (m/e 45) to diminish, when they are compared to the concentrations of d-$EtOD_2^+$ (m/e 54), CD_3-CD=OD^+ (m/e 50) and CD_2=C=OD^+ (m/e 46), respectively. The fact that the ratio, I_{46}/I_{45}, of the m/e 46 SSIMS intensity to the m/e 45 intensity is higher than the I_{50}/I_{49} and I_{54}/I_{52} ratios supports that there is an additional contribution to the m/e 46 intensity from $SiOD^+$ ions. The production of SiOH species during EtOH reactions with silicon dioxide is again confirmed.

Elimination of methyl via α-cleavage from deuterated ethanol yielded the deuterated counterparts of the species which contributed to the m/e31 signal shown in Fig. 7. The loss of CD_3 from d-EtOD yielded a stable oxonium, $CD_2=OD^+$, which, together with ethyl species, contributed to the signal intensity observed at m/e 34 in Fig. 8. Based on the discussion above, d-EtOH was also present on the surface when d-EtOD was exposed to the sample. The breakage of the C-C bond from d-EtOH produced another oxonium, $CD_2=OH^+$, which contributed to the signal intensity observed at m/e 33. The elimination of methyl from ethanol also led to the presence of the m/e 15 (CH_3^+) peak in the SSIMS spectrum shown in Fig. 7 and of the m/e 18 (CD_3^+) peak shown in Fig. 8 at high exposures. They all suggest that the C-C bond in ethanol may be disrupted.

Opposite to the intensities lopsided to the low-mass partner observed at 0.1L exposure of d-EtOD for the pairs of peaks (m/e 45 vs. m/e 46, m/e 49 vs. m/e 50, and m/e 52 vs. m/e 53) shown in the high mass region in Fig. 8, the SSIMS intensity obtained at m/e 33 was significantly smaller than that of m/e 34. As discussed above, the high-mass partners of these pairs of peaks may all originate from surface reactions of d-EtOD, and the low-mass one from that of d-EtOH. The previous discussion also indicates that the surface concentration of d-EtOH is higher than d-EtOD at 0.1L d-EtOD exposure. The observation of a smaller peak at m/e 33 than the peak at m/e 34 thus indicates that, when d-EtOD is exposed, ethyl species and its product from H/D exchange contribute substantially more to the intensities measured at m/e 33 and m/34 than the oxonium species. This conclusion is also consistent with the intensity difference displayed in Fig. 7 between m/e 29 and m/e 31.

TPD experiments were performed in which the desorption of the m/e 48 species was monitored in order to assure the occurrence of ethanol conversion to acetaldehyde on the sample surface. At d-EtOD exposure of 0.76L, the m/e 48 TPD spectrum exhibited a desorption feature peaking at the temperature of -48℃, which was 14℃ higher than the peak temperature of desorption measured at the same exposure for the m/e 52 (d-EtOD) species. Thus, the rise of the m/e 48 peak can not be attributed to the fragmentation of deuterated ethanol in the TPD ionizer. In comparison to the standard electron-impact mass spectrum of ethanol,[39] the observed larger peak intensity of desorption for m/e 48 than that for m/e 52, by about 10%, also excluded the possibility that m/e 48 was mainly formed in the ionizer due to the fragmentation of m/e 52.

Early studies[40,41] have shown that in the presence of silica samples preheated to above 820K, ethanol can be dehydrogenated at reaction temperatures of above 570K to yield acetaldehyde and hydrogen. A series of experiments carried out by Matsumura, et al.[42] in a pulse microcatalytic reactor showed that over the silica sample preheated at 1170K in vacuum for 30 min, as high as 100% selectivity may be achieved for the conversion of ethanol to acetaldehyde when the reaction temperature was lower than 570K, although the corresponding conversion rate was as low as 4%.[42] The conversion rate dropped to 0% at the reaction temperature of 520K. It maximized at 670K at an expense of the selectivity, i.e., ethylene and carbon residues were also produced. This study, however, showed that acetaldehyde can be formed at the reaction temperature of as low as –160℃ on the metal-free silicon dioxide sample prepared via thermal oxidation of silicon wafer and preheated to 700℃ in vacuum. The difference in the experimental results obtained may be partly due to the use of gas chromatography for analysis of reaction products in Matsumura‘s experiments.[42] The suppression in the acetaldehyde yield observed in this study at high ethanol exposures can be ascribed to the coverage of the sample surface at -160℃ by ethanol fragments and products.

As discussed above, the surface concentration of SiD increased quickly as the exposure of d-EtOD was increased. It may account for more than 50% of the signal intensity measured at m/e 30. The higher surface concentrations of D atoms at increasing d-EtOD exposures should suppress the rate of H/D exchange and result in a decrease in the yield of m/e 32 ($C_2D_3H_2^+$) species generated from deuterated ethyl ($C_2D_5^+$). Fig. 8, however, shows that the ratio, A_{32}/A_{34}, of the SSIMS peak area measured at m/e 32 (A_{32}) to that at m/e 34 (A_{34}) does not vary substantially with the exposure, especially after initial exposures of ethanol. In comparison to A_{33}/A_{34}, the magnitude of the A_{32}/A_{34} ratio also do not agree with the kinetics of H/D exchange, which predicts a significantly smaller rate for consecutive exchanges (i.e., for m/e 34 to generate m/e 32) than for single exchange (i.e., for m/e 34 to generate m/e 33).

The relative selectivity of the sample surface for ethanol conversion to produce ethylene and acetaldehyde at low substrate temperature of –160℃ can be roughly estimated. As discussed before, the contribution of d-EtO$^+$ ions to the m/e 50 peak intensity shown in Fig. 8 is minimal. Instead, the m/e 50 peak originates mainly from the sputtering of CD_3-CD=OD$^+$ ions. The sum of the peak areas measured at m/e 49 (CD_3-CD=OH$^+$) and m/e 50 may thus represent, to some extent, the quantity of acetaldehyde produced on the surface. In addition, the peak area obtained at m/e 32 (Fig. 8) may reflect the production of ethylene on the surface because of the expected low yield from consecutive H/D exchanges. The dependence on the exposure of ethanol conversion to ethylene and acetaldehyde over silicon dioxide can then be investigated by assuming that the ionization probabilities of ethylene and acetaldehyde under ion bombardment for SSIMS detection are similar, since the ionization energy for acetaldehyde is 10.22 eV[43,44] and that for ethylene is 10.51 eV.[45,46] As shown in Fig. 11A, the sputter yields, relative to the Si$^+$ (m/e 28) yield, of both ethylene (m/e 32) and acetaldehyde (m/e 49 and m/e 50) increase rapidly with the ethanol exposure. Although the Si$^+$ yield is expected to decrease with the exposure because of the surface coverage, which may cause the relative yields to increase somewhat, the observed rapid increase indicates that the silicon dioxide surface is reactive for ethanol conversion in the exposure range studied. Both dehydrogenation to produce acetaldehyde and dehydration to yield ethylene can take place on the surface at the low substrate temperature of –160℃.

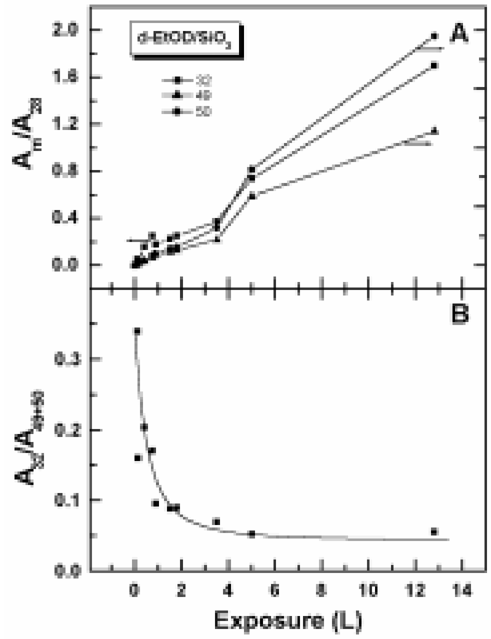

Fig. 11 A) Ratios of peak areas obtained at m/e 32, 49, and 50 to the area of the m/e 28 peak in the SSIMS spectra of a silicon dioxide surface exposed to d-EtOD. B) Ratio of the area of the m/e 32 peak to the sum of the peak areas obtained at m/e 49 and 50 in the SSIMS spectra of a silicon dioxide surface exposed to d-EtOD. All measurements were taken at –160 ℃.

The selectivity of the sample surface for these two reactions, however, does not remain constant in the exposure range studied. Fig. 11B shows the ratio of the SSIMS peak area for ethylene to that for acetaldehyde as a function of ethanol exposure. As the exposure is increased, the ratio decreases rapidly from 0.35 at 0.12 L exposure to 0.1 at ~1.5L exposure. Further increase in exposure does not cause the ratio to change drastically. The figure shows that, for ethanol reactions on silicon dioxide at –160℃, more ethylene is produced on the bare surface than that at high exposures, although the production of acetaldehyde is favored over that of ethylene in the entire range of exposure studied. The selectivity towards dehydrogenation of ethanol in the presence of silicon dioxide increases with the exposure, with the ethylene yield amounting to ~5% of the acetaldehyde yield at high exposures

Other studies performed on dehydrated silica also observed the production of ethylene from ethanol. Thermogravimetry-mass spectroscopy studies[32] of silica calcined at more than 500℃ before being exposed to ethanol showed the formation of ethylene at 550℃ after ethanol was introduced. Analysis with gas chromatography of the products generated from ethanol exposure to a silica sample pretreated at 1170K showed no production of ethylene until the reaction temperature was raised to above 620K.[40,42] The selectivity for ethanol dehydration became greater, along with the total rate of conversion, at higher reaction temperatures.[40,42] In contrast, this study showed that dehydration may take place on the bare silicon dioxide surface at low reaction temperature of –160℃. Figs. 7 and 8 show that its product, ethylene, however, accounts for a very small portion of the products yielded from ethanol reactions on silicon dioxide. The selectivity for ethylene formation also drops rapidly with the ethanol dose. Not until at high substrate temperatures would ethylene become the dominant product and was then detected by the analytical techniques employed in other studies.[30-32,40,42]

The presence of surface strains on the sample surface was supported by the relatively large SSIMS intensity observed at m/e 44 (SiO^+) in Figs. 7 and 8. As mentioned above, the area of the m/e 44 peak obtained from the clean surface amounted to ~19% of the one measured at m/e 28. This value was higher than the expected one for the desorbed Si and O atoms which were ejected from the silicon dioxide surface via certain correlated collision sequences.[23-25] Thus, the formation of the SiO species during sputtering cannot be explained entirely by the recombination reactions above the surface. It is postulated that the strain developed in the siloxane bridges on the sample surface may facilitate sputtering of SiO from the sample. Quantum-chemical calculations of cluster models of silica surfaces showed that condensation of silanol groups led to the formation of strained siloxane bridges on the surface.[47] Strains were developed in these bridges upon condensation due to the distortion of the bridge bond angles away from that of tetrahedron[48] and to the restructuring of the silica matrix in the vicinity of these bridges.[49,50] The silanol surface population of 2.6±0.5 OH/nm^2 obtained above thus implied that the sample surface prepared in this study must contain strained siloxane bridges, which were produced via condensation of silanols during sample preparation and repeated annealing at 700℃. The presence of strains and silanols on the sample surface, in turn, accounts for the large reactivity of the bare, metal-free silicon dioxide surface observed in this study toward ethanol decomposition.

As observed by Atanassova et al.,[39] ethanol reactions with the silicon dioxide surface introduced defects in the silicon-silicon dioxide structure. The defects were a source of electrically active centers, which may lead to an increase in the charge density in the dielectric layer and at the interfaces under the drain voltage.[39,51-53] Their studies[39] showed that after the interaction of ethanol vapors with the silicon dioxide surface, the charge density increased from <10^9 cm^{-2} to (1.5-1.7) x 10^{11} cm^{-2}. The surface charge on the oxide was mainly responsible for the ethanol–induced positive charge in the silicon-silicon dioxide structure.[51,39] It was proposed that the surface charge was produced as a result of molecular polarization due to ethanol adsorption on the surface and of the generation and diffusion of the products formed from ethanol surface reactions.[39] The observation of the weak dependence[39] of the charge density on the level of surface saturation in ethanol vapor showed that the leakage current was limited mainly by the surface chemical reaction, rather than the diffusions of the products and the possible chemical changes due to this diffusion.

References

1. H. Miguez, C. Lopez, F. Meseguer, A. Blanco, L. Vazquez, R. Mayoral, M. Ocana, V. Fornes, A. Mifsud, *Appl. Phys. Lett.* **71** (1997) 1148.
2. S. Kawakami, *Electron. Lett*. **33** (1997) 1260.
3. S. Kawakami, T. Kawashima, T. Sato, *Appl. Phys. Lett*. **74** (1999) 463.
4. H. Miguez, F. Meseguer, C. Lopez, A. Mifsud, J. S. Moya, L. Vazquez, *Langmuir* **13** (1997) 6009.
5. B. Cheng, P. Ni, C. Jin, Z. Li, D. Zhang, P. Dong, X. Guo, *Optics Comm*. **170** (1999) 41.
6. H. S. Sozuer, J. W. Haus, R. Inguva, *Phys. Rev*. **B45** (1992) 13962.
7. H. Miguez, C. Lopez, F. Meseguer, A. Blanco, L. VazQuez, R. Mayoral, M. Ocana, A. Mifsud, V. Fornes, *Appl. Phys. Lett*. **71** (1997) 1148.
8. H. Miguez, F. Meseguer, C. Lopez, A. Blanco, J. S. Moya, J. Requena, A. Mifsud, V. Fornes, *Adv. Mater*. **10** (1998) 480.
9. R. Mayoral, J. Requena, J. S. Moya, C. Lopez, A. Cintas, H. Miguez, F. Meseguer, L. Vazquez, M. Holgado, A. Blanco, *Adv. Mater*. **9** (1997) 257.
10. V. N. Astratov, Yu. Vlasov, O. Z. Karimov, A. A. Kaplyanskii, Yu. Musikhin, N. A. Bert, V. N. Bogomolov, A. V. Prokofiev, *Phys. Lett*. **A222** (1996) 349.
11. H. Miguez, F. Meseguer, C. Lopez, A. Blanco, J. S. Moya, J. Requena, A. Mifsud, V. Fornes, *Adv. Mater*. **10** (1998) 480.
12. H. Miguez, F. Meseguer, C. Lopez, A. Blanco, J. S. Moya, J. Requena, A. Mifsud, V. Fornes, *Adv. Mater*. **10** (1998) 480.
13. J. E. G. J. Wijnhoven, W. L. Vos, *Science* **281** (1998) 802.
14. Chang, C.-C.; Huang, I.-J.; Lung, C.-H.; Hwang, H.-Y.; Teng, L.-Y. *J. Phy. Chem.* **2001**, *105*, 994.
15. Ishizaka, A.; Shiraki, Y. *J. Electrochem. Soc.* **1985**, *133*, 666.
16. Harrison, D. E., Jr.; Kelly, P. W.; Garrison, B. J.; Winograd, N. *Surf. Sci.* **1978**, *76*, 311.
17. Chang, C.-C.; Winograd, N. *Phys. Rev.* **1989**, *39*, 3467.
18. Chang, C.-C.; Hsieh, J.-Y. *Phys. Rev.* **1998**, *B57*, 12564.
19. Ballinger, T. H.; Yates, J. T., Jr. *Langmuir* **1991**, *7*, 3041.
20. Knozinger, H. *Surface Organometallic Chemistry: Molecular Approaches to Surface Catalysis*; Basset, J.-M. Ed.; Kluwer Academic Publishers: New York, 1988, p. 35-46.
21. Boehm, H.-P.; Knozinger, H. *Catal. Sci. Technol*; Anderson, J. R.; Boudart M., Eds.; *Vol. 4* Springer: Berlin, 1983, p. 40-189.
22. Zaki, M. I.; Hasan, M. A.; Al-Sagheer, E. A.; Pasupulety, L.; *Colloids Surf.* **2001**, *190*, 261.
23. Winograd, N.; Harrison, D. E., Jr.; Garrison, B. J. *Surf. Sci.* **1978**, *78*, 467.
24. Ivanov, V. P.; Trukhan, S. N.; Borodin, A. I. *International J. Mass Spectr.* **1999**, *188*, 183.
25. Chang, C.-C. *Phys. Rev.* **1993**, *B48*, 12399.
26. Revesz, A. G. *J. Electrochem. Soc.* **1979**, *126*, 122.
27. *Saracual, A. R. A.; Pulton, S. K.; Vicary, G.; Rochester, C.* J. Chem. Soc. Faraday Trans. ***1982***, I78, *2285.*
28. Plueddermann, E. P. *Silane Coupling Agents*; Plenum Press: New York, 1982.
29. Curtiss, L. A.; Lucas, D. J.; Pople, J. A. *J. Chem. Phys.* **1995**, *102*, 3292.
30. Crowell, J. E.; Tedder, L. L.; Cho, H.-C.; Cascarano, F. M.; Logan, M. A. *J. Vac. Sci. Technol.* **1990**, *A8*, 1864.
31. Tedder, L. L.; Lu, G.; Crowell, J. E. *J. Appl. Phys.* **1991**, *69*, 7037.
32. Ho, S.-W.; Su, Y.-S. *J. Catal.* **1997**, *168*, 51.

33. Little, L. H. *Infrared Spectra of Adsorbed Species*; Academic Press: New York, 1966.
34. Ramond, T. M.; Davico, G. E.; Schwartz, R. L.; Lineberger, W. C. *J. Chem. Phys.* **2000**, *112*, 1158.
35. Dang, T. T.; Motell, E. L.; Travers, M. J.; Clifford, E. P.; Ellison, G. B.; Depuy, C. H.; Bierbaum, V. M. *Int. J. Mass Spectrom. Ion Processes* **1993**, *123*, 171.
36. Ruscic, B.; Berkowitz, J. *J. Chem. Phys.* **1994**, *101*, 10936.
37. Mizukami, M.; Kurihara, K. *Chem. Lett.* **2000**, 256.
38. Silverstein, R. M.; Bassler, G. C.; Morrill, T. C. *Spectrometric Identification of Organic Compounds*, 5ed.; New York: Wiley, 1991.
39. Atanassova, E.; Dimitrova, T. *Solid-St. Electron.* **1993**, *36*, 1711.
40. Matsumura, Y.; Hashimoto, K.; Yoshida, S. *J. Chem. Soc. Chem. Commun.* **1987**, 1599.
41. Matsumura, Y.; Hashimoto, K.; Yoshida, S. *J. Catal.* **1990**, *122*, 352.
42. Matsumura, Y.; Hashimoto, K.; Yoshida, S.; *J. Catal.* **1989**, *117*, 135.
43. Traeger, J. C. *Int. J. Mass Spectrom. Ion Processes* **1985**, *66*, 271.
44. Hernandez, R.; Masclet, P.; Mouvier, G. *J. Electron Spectrosc. Relat. Phenom.* **1977**, *10*, 333.
45. Ohno, K.; Okamura, K.; Yamakado, H.; Hoshino, S.; Takami, T.; Yamauchi, M. *J. Phys. Chem.* **1995**, *99*, 14247.
46. Williams, B. A.; Cool, T. A. *J. Am. Chem. Soc.* **1991**, *94*, 6358.
47. Lygin, V. I. *Zh. Fiz. Khim.* **1989**, *63*, 289.
48. Fink, M. J.; Haller, K. J.; West, R.; Michl, J. *J. Am. Chem. Soc.* **1984**, *106*, 822.
49. Morrow, B. A.; Devi, A. *Trans. Faraday Soc.* **1972**, *68*, 403.
50. Bunker, B. C.; Haaland, D. M.; Ward, K. J.; Michalske, T. A.; Smith, W. L.; Binkley, J. S.; Melius, C. F.; Balfe, C. A. *Surf. Sci.* **1989**, *210*, 406.
51. DiMaria, D. J.; Cartier, E.; Arnold, D. *J. Appl. Phys.* **1993**, *73*, 3367.
52. Blochl, P. E.; Stathis, J. H. *Physica* **1999**, *B273*, 1022.
53. Blochl, P. E.; Stathis, J. H. *Phys. Rev. Lett.* **1999**, *83*, 372.